Next Materials 2 (2024) 100125

Contents lists available at ScienceDirect

Next Materials

journal homepage: www.sciencedirect.com/journal/next-materials

Research article

Crude glycerol esterification using biomass-derived carbon acid catalysts

Federico M. Perez [a,b], Martín N. Gatti [a,b], Carla S. Fermanelli [c], Clara Saux [c], M. Soledad Renzini [c], Francisco Pompeo [a,b,*]

[a] CINDECA, Facultad de Ciencias Exactas, Universidad Nacional de La Plata, CCT La Plata, CONICET, 47 N° 257, 1900 La Plata, Argentina
[b] Departamento de Ingenieria Quimica, Facultad de Ingeniería, Universidad Nacional de La Plata, 1 esq 47, 1900 La Plata, Argentina
[c] Centro de Investigación y Tecnología Química (CITeQ), UTN – CONICET, Maestro López esq. Cruz Roja Argentina, 5016 Córdoba, Argentina

ARTICLE INFO

Keywords:
Crude glycerol
Esterification
Acid catalysts
Biochar
Biomass
Biorefineries

ABSTRACT

In this work, carbons obtained from peanut shells (PC), activated with KOH (APC) and functionalized with H_2SO_4 (PC-F and APC-F, respectively) were evaluated as catalysts in the esterification of crude glycerol with acetic acid to obtain monoacetyl glycerol, diacetyl and triacetyl glycerol. The characterization revealed that both PC-F and APC-F have high specific surface areas and very strong acid sites due to the presence of -HSO_3 groups. The activity of both catalysts was evaluated using crude glycerol obtained from biodiesel synthesis, which presented acid pH, water, methanol, Na_2SO_4 and non-glycerol organic matter (MONG) as major impurities. The APC-F catalyst was more active than PC-F due to the combination of its surface acidity and textural properties. After 5 reaction cycles at 120 °C, using an acetic acid/glycerol molar ratio of 6 and a catalyst/glycerol mass ratio of 0.25, APC-F showed a decrease in specific surface area and pore volume due to the adsorption of Na_2SO_4 present in the crude glycerol. However, it was able to maintain activity levels with 100% glycerol conversion and selectivity to monoacetyl glycerol, diacetyl glycerol and triacetyl glycerol of 55%, 35% and 10%, respectively.

1. Introduction

In recent years, the growing energy demand has led scientists to investigate new forms of energy that, in addition to enabling economic and social development, are eco-compatible and sustainable over time. In this context, biomass resources originated from natural and renewable organic supplies serve as energy sources and allow the production of high value-added products such as fine chemicals, materials, and other consumer goods [1].

Among all the possible biomass conversion processes, the production of liquid biofuels is one of the most developed valorization routes at the international level, mainly exploited by countries with high biomass availability [2]. Among biofuels, biodiesel derived from soybean oil, and bioethanol derived from sugarcane and corn are the two most widely used types of biofuels in the world.

Biodiesel production generates approximately 1 kg of glycerin as a by-product for every 10 kg of biofuel. Its wide availability and relatively low cost as a raw material have made glycerol an economical feedstock for the production of various chemical products, such as hydrogen [3], cyclic acetals [4] and glycols with high added value [5,6], which allows the development of biorefineries around biodiesel plants through the technological integration with the processes already installed in these plants.

The use of glycerol in combustion engines has gained much attention in recent years, since returning it to fuels means taking advantage of its energy content and reducing emissions during combustion. Regarding the use of glycerin as a fuel, its direct incorporation into internal combustion engines presents difficulties due to its low calorific value, high viscosity, and high auto-ignition temperature. Because of this, it is necessary to address these difficulties to effectively utilize glycerol as a fuel source. In this sense, several reactions have been studied to convert glycerol into fuel additives that improve its properties, such as etherification, esterification, acetalization-ketalization, and transesterification [7].

Abbreviations: MAG, monoacetyl glycerol; DAG, diacetyl glycerol; TAG, triacetyl glycerol; X, glycerol conversion; S_i, selectivity towards product i; C, carbon balance; G, glycerol; W, water; AA, acetic Acid; MeOH, methanol; MONG, non-glycerol organic matter; AA/G, acetic acid/Glycerol molar ratio; S_{BET}, specific Surface Area obtained by BET equation; V_p, total pore volume; V_{micro}, micropore volume; V_{meso}, mesopore volume; E_i, initial potential; NS, total number of acid sites; PC, pyrolytic carbon; APC, activated pyrolytic carbon; PC-F, functionalized pyrolytic carbon; APC-F, functionalized activated pyrolytic carbon.

* Corresponding author at: CINDECA, Facultad de Ciencias Exactas, Universidad Nacional de La Plata, CCT La Plata, CONICET, 47 Nº 257, 1900 La Plata, Argentina
E-mail address: fpompeo@quimica.unlp.edu.ar (F. Pompeo).

https://doi.org/10.1016/j.nxmate.2024.100125
Received 31 July 2023; Received in revised form 11 January 2024; Accepted 15 January 2024

The esterification of glycerol with acetic acid has gained great importance in recent years. This reaction yields monoacetyl glycerol (1-MAG and 2-MAG), diacetyl glycerol (1,2-DAG and 1,3-DAG) and triacetyl glycerol (TAG) (Scheme 1).

In particular, MAGs are used as additives in the pharmaceutical and food industries and in the manufacture of explosives. DAGs are found in cocoa butter and are used as intermediates in the structural synthesis of lipids [8]. With regard to TAG, its use in the production of cosmetics, plasticizers and solvents has been reported. In addition, the FDA (Food and Drug Administration) considers it a GRAS (Generally Recognized As Safe) additive, so it is used as a flavoring agent, humectant, and solvent in foods [9]. In particular, the high O/C ratio in DAG and TAG molecules makes them promising additives for fuels, improving their performance, facilitating their transport at low temperatures, and reducing the emission of harmful gases during their combustion. This would make it possible to replace the current petrochemical-based antiknock agents, methyl tert-butyl ether and ethyl tert-butyl ether [10,11]. Unlike these ethers, acetylglycerols are a better option because they are non-toxic, biodegradable and renewable [2].

Furthermore, it is important to remark that the esterification of glycerol with acetic acid is carried out in the liquid phase according to the Fischer esterification mechanism, either in the presence of homogeneous catalysts or in their absence, with acetic acid itself being the autocatalytic agent [12]. In the former case, organic and inorganic acids such as p-toluensulfonic acid [13] and H_2SO_4 [14,15] have been used. However, the toxicity and corrosiveness of these acids cause certain disadvantages in the design and operation of the equipment [16–18].

To overcome these drawbacks, heterogeneous catalysts based on acidic Brønsted solids that follow a reaction mechanism similar to that reported by Fischer [19,20] have been used. In this sense, several solids have been reported in the literature, such as ion exchange resins [21], zeolites [22], activated clays [23], inorganic oxides [24], heteropolyacids [25], and functionalized mesoporous materials [26]. Among them, biomass-derived carbons are an interesting, inexpensive, and environmentally friendly alternative. The wide variety of carbon sources, together with the different strategies to provide them with acid sites, generates a wide variety of catalysts. Among the biomass sources commonly used for the preparation of coals, solid biomass residues such as seed shells, grains and bunches are the most interesting ones.

According to the United States Department of Agriculture (USDA), world peanut production exceeds 50 million tons per year [27]. It should be noted that 25% of the production corresponds to the shell of this legume, which has no commercial value. In addition, its low density and high combustion capacity represent disadvantages for its storage. In recent years, the thermochemical treatment of biomass waste, e.g. through pyrolysis, has become increasingly significant since it offers a means to dispose of this waste while simultaneously enabling the synthesis of value-added compounds. The solid formed during pyrolysis, known as "biochar", can be used as a solid fuel, catalyst, adsorbent, etc. and, therefore, the use of peanut shell for the production of carbonaceous materials represents significant economic and environmental benefits [28,29].

Activity results using these catalytic systems have revealed that both glycerol conversion and acetylglycerols selectivity depend on the reaction conditions, such as temperature, AA/G molar ratio, initial water content in solution and reaction time. These conditions depend on the nature of the catalyst and its concentration in the reaction medium [30].

Most recent articles on catalysts based on biomass-derived carbons have reported satisfactory activity but utilizing analytical-grade glycerol as a reagent [31–34]. Investigating the performance of catalysts using crude glycerol is vital since refining crude glycerol can result in substantial costs that may adversely impact process profitability and the final product price. In order to reach industrial scale viable operating conditions, it is required to use glycerol in concentrations similar to those of crude glycerol, which are above that range (50–80 wt%). In the present article, we evaluate the performance of a catalyst based on crude

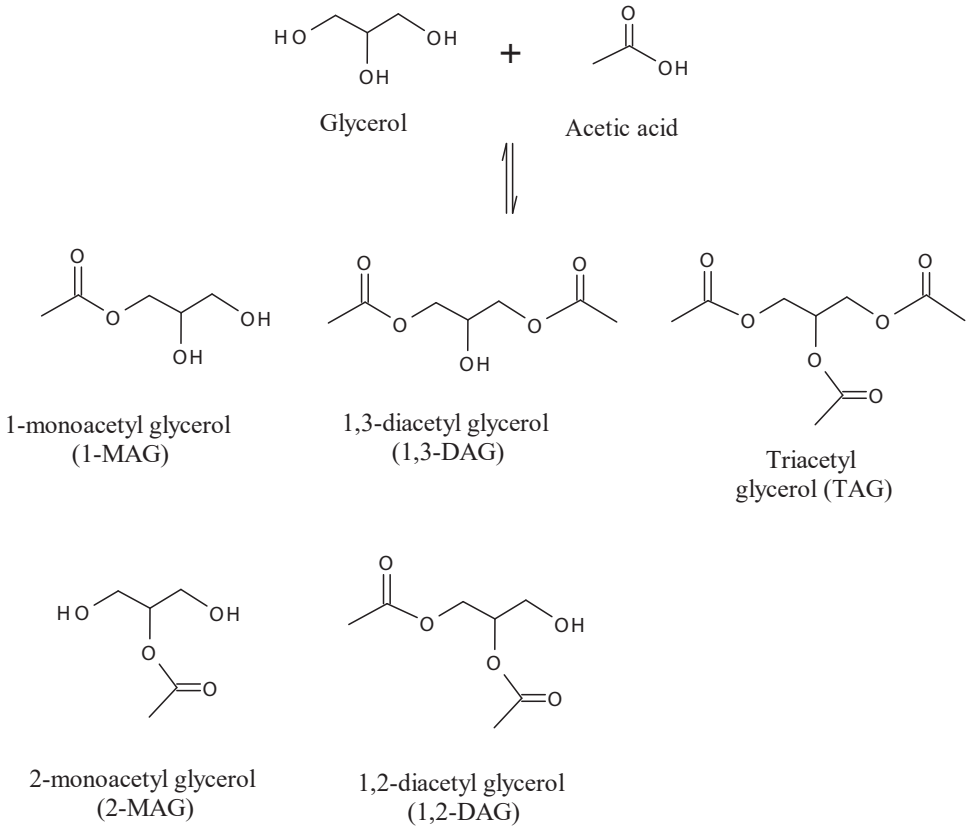

Scheme 1. Esterification of glycerol with acetic acid to produce monoacetyl glycerol, diacetyl glycerol and triacetyl glycerol.

glycerol coming directly from the Argentine biodiesel industry, which we consider to be a novel contribution to this field.

Crude glycerol contains a large number of impurities, including inorganic bases, sodium or potassium salts, methanol (MeOH) and residues and non-glycerol organic matter (MONG) such as free fatty acids, residues of oils and fats that have not reacted in the biodiesel synthesis process [35–37]. The nature of these impurities and their concentration can have, to a greater or lesser extent, a different impact on the production of acetylglycerols.

In this context, the objective of this work is to evaluate carbons obtained from residual biomass of high production volume (peanut shells) as catalysts in the esterification reaction of crude glycerol with acetic acid.

2. Experimental

2.1. Catalyst preparation

The carbons used as catalysts in the esterification process were obtained from peanut shells provided by the Lorenzati, Ruetsch y Cía S.A. company (Córdoba, Argentina). Since it is a creeping fruit with a high content of physically adhered soil, the biomass was previously washed with water and dried in an oven at 105 °C until constant weight, in order to eliminate any impurities. It was then subjected to a pyrolysis process at 500 °C in a fixed-bed reactor under N_2 flow (60 ml min^{-1}) for 10 min. The solid product of this procedure was called pyrolytic carbon (PC).

In order to increase its surface area and pore diameter, this material was subjected to a physicochemical activation process. This consisted of a mechanical mixture of PC with KOH (1:3 mass ratio), followed by heating at 550 °C under N_2 flow and subsequent washing with distilled water until neutral pH. This material was called activated pyrolytic carbon (APC).

As a last step, to provide these materials with the acid sites necessary for the reaction, they were functionalized with H_2SO_4. For this purpose, 1 g of carbon was mixed with 25 ml H_2SO_4 (98 wt%) under continuous stirring at 140 °C for 24 h. Subsequently, the solids were washed with distilled water to neutral pH and dried in an oven for 24 h at 110 °C. The solids finally obtained were named PC-F and APC-F.

2.2. Catalyst characterization

Textural characterization was carried out by N_2 adsorption-desorption measurements at − 196 °C using the Brunauer-Emmett-Teller (BET) multipoint method, employing an ASAP 2020 Plus 2.00 equipment. Prior to analysis, the samples were degassed at 300 °C.

X-ray diffractograms were obtained employing a Panalytical X'Pert PRO powder diffractometer, using CuKα radiation (λ = 1.5418 Å, intensity = 20 mA and voltage = 40 kV). The patterns were recorded in the range 2θ = 5°− 80 °.

The acid strength and total number of acid sites were determined by the potentiometric titration technique employing a Metrohm 794 Basic Titrino apparatus with a double junction electrode. For each assay, 0.05 g of sample were suspended in pure acetonitrile (Merck) and shaken for 3 h prior to analysis. The suspensions were then titrated with a 0.05 N solution of n-butylamine (Carlo Erba) in acetonitrile.

The Fourier Transform Infrared spectra of the catalysts were obtained using a Nicolet Model iS10 instrument. The materials were analyzed in tablet form, made by pressing a mixture of anhydrous KBr and the substance to be studied, under a pressure of 8 MPa. The analysis was performed in a wavenumber range of 4000–500 cm^{-1}.

Laser Raman spectra (LRS) were recorded employing a LabRam spectrometer (Horiba-Jobin-Yvon) coupled to a 100 × objective lens (Olympus confocal microscope), used for simultaneous illumination and collection. The spectrometer was equipped with a CCD detector cooled to 200 K. A 532 nm edge laser (Spectra Physics diode-pumped solid-state laser) was used for the continuous scanning. The laser power was 30 mW. Each sample was examined at different locations to confirm the results.

The X-ray photoelectron spectra were obtained employing a Thermo Scientific K-Alpha model equipment (LAMARX-FAMaF-UNC). This is an XPS system with a monochromatic X-ray source, capable of high-resolution, small-area XPS analysis, line scans, chemical mapping and in-depth compositional profiling of both conductive and insulating samples. C 1 s at 284.6 eV was used as a charging reference and spectra were analyzed with the CasaXPS software.

2.3. Crude glycerol characterization

Crude glycerol was supplied by SEIBO-Ingeniería S.A. (Buenos Aires-Argentina). It was characterized for density, pH and concentration of glycerol, water, methanol, ash and MONG.

Density was determined using a pycnometer at room temperature (ASTM 891–95). The pH was determined using 1 g of crude glycerol dissolved in 50 ml of distilled water using a digital pH meter Ohaus ST20 at room temperature. Glycerol and methanol concentrations were determined using dilute solutions of Crude Glycerol by gas chromatography, employing a Shimadzu GCMS-QP505A instrument equipped with an Elite PE-WAX capillary column (30mx 0.25 mm×0.5 μm) and FID detector. The water content was measured using a Karl-Fisher titrator according to ISO 2098–1972. The ash content was determined by burning 1 g of crude glycerol in a muffle furnace at 750 °C for 3 h (ISO 2098–1972). The MONG content was calculated as shown in Eq. (1).

$$\text{MONG}\ (\%) = 100 - \text{glycerol content}\ (\%) - \text{ash content}\ (\%) - \text{water content}\ (\%) \quad (1)$$

2.4. Catalytic activity

The reaction tests were carried out in a BR-100 (Berghof, Eningen, Germany) high-pressure stainless-steel batch reactor of 100 ml. Magnetic stirring was set at 1000 rpm to ensure kinetic control in all tests.

In a typical experiment, crude glycerol, acetic acid and the catalyst were loaded into the reactor, using acetic acid/glycerol molar ratios (AA/G) between 1 and 9. Then, the reactor was pressurized to 2 MPa with N_2 and heated to the desired temperature (80–200 °C). Some tests were carried out employing glycerol of analytical grade (99.99%p/p, Cicarelli).

The identification and quantification of the reaction products were carried out by gas chromatography employing a Shimadzu GCMS QP5050A instrument equipped with a PE-Elite-Wax capillary column (30 m × 0.25 mm × 0.5 μm, purchased by Perkin Elmer, and an FID MS detector, using n-propanol (Anedra) as external standard.

The glycerol conversion was determined according to Eq. (2).

$$X\ (\%) = \frac{\text{moles of consumed glycerol}}{\text{moles of initial glycerol}} 100\ \% \quad (2)$$

The selectivity towards the product *i* was determined according to Eq. (3).

$$S_i\ (\%) = \frac{\text{moles of product i}}{\text{total moles of products}} 100\ \% \quad (3)$$

The carbon balance was calculated using Eq. (4).

$$C\ (\%) = \frac{\text{total moles of carbon in the products}}{\text{3. moles of initial glycerol} + \text{2. moles of initial acetic acid}} 100\ \% \quad (4)$$

The accuracy of the measurements was within 5%, and the experiments could be reproduced with a relative error of 10%.

3. Results and discussion

3.1. Catalyst characterization

Firstly, the textural properties of the synthesized solids were determined using the N_2 adsorption-desorption technique. The results are shown in Table 1.

The activation treatment resulted in a significant increase in the surface area of APC with respect to PC (692 and 215 $m^2\ g^{-1}$, respectively). This can be attributed to the unblocking of structural pores due to the effect of KOH and the heat treatment applied [38]. In addition, the functionalized materials present a higher specific surface area than the starting materials, indicating that the acid treatment generates new pores and releases some occluded pores of the carbonaceous solid [39]. This phenomenon may be a result of the cleavage of the glycosidic bond of cellulose and hemicellulose in APC during sulfonation, leading to an increase of the specific surface area in APC-F [40]. Similar results were obtained by Wei et al., who prepared carbon-based solid acid catalysts by sulfonation of rice straw pyrolytic carbon at 80 °C [41].

The X-ray diffraction spectra of the PC and APC solids are shown in Fig. 1.

In the above figure, two broad peaks are observed near $2\theta = 20°$ and 45° (*), which are attributed to graphitic planes (002) and (101), respectively. It is important to mention that the H_2SO_4 treatment does not generate changes in the crystalline structure of the PC and APC carbons, so that only the spectra of the starting materials are shown in Fig. 1.

The strength and number of acid sites present in the catalysts are important parameters that determine the activity of the catalysts in the esterification reaction of glycerol with acetic acid, which were determined by the potentiometric titration technique with N-butylamine. The initial electrode potential (E_i) indicates the acidic strength of the sites, according to the following scale: very strong, Ei> 100 mV; strong, 0 <Ei< 100 mV; weak $-100 < Ei < 0$ mV, and very weak, Ei< −100 mV [42]. Firstly, the PC and APC catalysts present a similar number of acid sites (0.43 and 0.40 mmol g^{-1}, respectively) and both possess strong acid sites ($0 < Ei < 100$ mV). On the other hand, an increase in the total number of acid sites is observed in the functionalized materials, as shown in Table 1, indicating that the H_2SO_4 treatment is effective in acidifying the materials. Moreover, it can be observed that both solids undergo a considerable increase in the acidic strength of the sites after functionalization, since their initial potentials are above 100 mV.

To determine the nature of the acid sites generated by the treatment with H_2SO_4, and to establish the functional groups present in the solids, the Fourier Transform Infrared spectroscopy technique was used, whose spectra are shown in Fig. 2. In all the carbonaceous materials, the signal corresponding to O-H stretching at 3400 cm^{-1} can be clearly observed. This band is usually related to adsorbed water although it can also be assigned to the presence of phenol and carboxyl groups [43]. Zhang et al. [44] ascribed the signal at 2921 cm^{-1} to the C-H stretching vibration in aromatic rings. This signal suffered a slight reduction when the carbon was subjected to activation treatment and subsequent functionalization (APC-F), indicating a reduction in the cellulose content of this material [45]. On the other hand, the signal at 1586 cm^{-1} corresponding to the C═C bending in the aromatic rings increases its intensity in the functionalized samples (PC-F and APC-F) [46].

As shown in Fig. 2, the signal at 1050 cm^{-1} (associated with asymmetric C-O-C stretching) is notorious in all samples. However, in the case of APC-F, its intensity is considerably lower, confirming the lesser proportion of cellulose and hemicellulose in this material, due to the more complex physicochemical treatment.

The signals related to the sulfonic groups can be clearly observed in the spectra obtained for the PC-F and APC-F samples. A signal at 1705 cm^{-1} corresponding to the C═O vibration in the -COOH group, and the bands at 1171 and 1029 cm^{-1} associated with the symmetric stretching -SO_3H and O═S═O, respectively, can be clearly seen in these

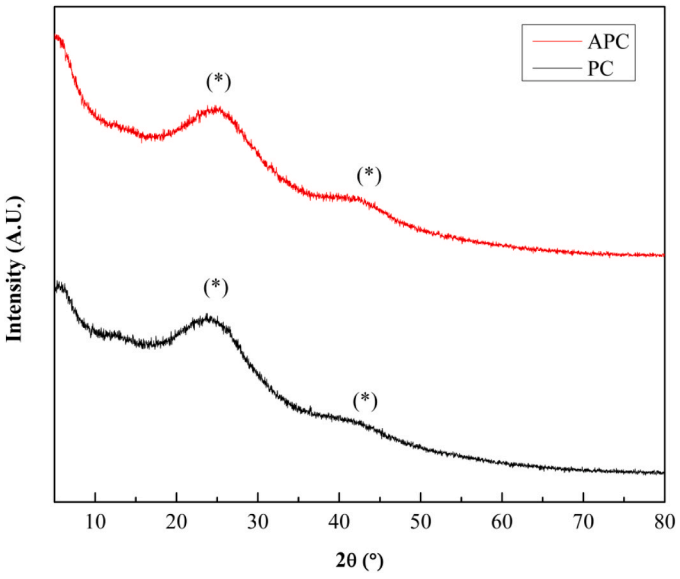

Fig. 1. X-ray diffraction spectra of the PC and APC samples.

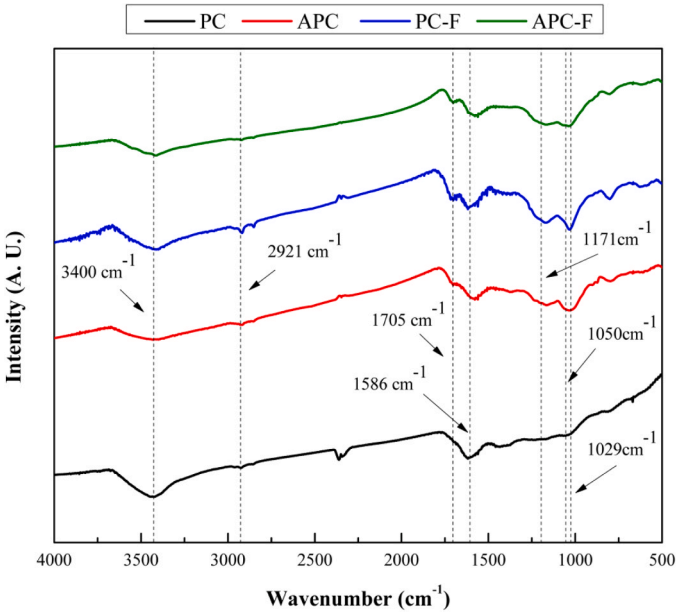

Fig. 2. Fourier Transform Infrared spectra of the starting materials (PC and APC) and the functionalized solids (PC-F and APC-F).

Table 1
Textural properties and acidity of solids.

Sample	Textural properties				Potentiometric titration	
	S_{BET} ($m^2\ g^{-1}$)	V_p ($cm^3\ g^{-1}$)	V_{micro} ($cm^3\ g^{-1}$)	V_{meso} ($cm^3\ g^{-1}$)	E_i (mV)	NS (mmol g^{-1})
APC	692	0.32	0.25	0.07	25.0	0.40
PC-F	448	0.17	0.15	0.02	375.4	1.10
APC-F	918	0.36	0.30	0.06	387.4	0.95
APC-F-Used	307	0.12	0.10	0.02	255.1	0.94

S_{BET}: specific surface area; V_p: total pore volume; V_{micro}: micropore volume; V_{meso}: mesopore volume; E_i: initial potential; NS: total number of acid sites.

spectra [47]. These results demonstrate that the applied functionalization treatment was efficient to incorporate covalently bonded -SO_3H functional groups into the carbon structure.

Raman spectra (Fig. 3) were obtained to determine the molecular structural characteristics of the catalysts. From the figure it is possible to observe the presence of the defect band (D-band) and graphitic bands (G-band) in all the samples, which are indicated on the spectra. These both characteristic signals of biochars are located around 1370 cm^{-1} (D-band) and 1590 cm^{-1} (G-band) but could vary according to biomass source [48]. Spectra were recorded from 500 to 3200 cm^{-1} and no other significant signals were observed. Curve fitting was performed using a Gaussian function for both bands.

The D-band is usually attributed to the disordered graphite ring of the samples, while the G-band is mainly due to the aromatic rings and the graphite crystallite [49,50]. As observed in the spectra, there is a relative increase in the G-band in activated biochars (APC and APC-F). Potgieter-Vermaak et al. attributed this behavior to an increase in carbon order, which is typical for biochar with lower volatile content [51]. The use of KOH and high temperature in the activation process induces their loss.

In addition, two bands located at ~1250 cm^{-1} (D*) and ~1550 cm^{-1} (D**) are observed in the activated carbons, which have been associated with carbon double bond stretching and hydrogen-carbon wagging modes, respectively, suggesting that these samples contain a large number of defects, possibly generated during the activation process [52,53].

Additionally, characterization tests were carried out using the X-ray photoelectron spectroscopy technique. Fig. 4 shows the spectra of the S2p, C1s and O1s region for the functionalized samples. In both samples a signal is observed at 168.5 eV (Fig. 4(a) and 4 (b)), indicating the presence of sulfur in its oxidized form (-SO_3H), confirming the presence of sulfonic groups, in agreement with the Fourier Transform Infrared spectroscopy technique [54–56].

With respect to the C1s region (Fig. 4(c) and 4 (d)), a main peak centered at 284.6 eV is observed, which corresponds to sp^2-hybridized graphitic carbon (C═C/C-C groups) [57]. Additionally, the peak observed at 285.7 eV can be assigned to -C-O groups (C associated with ether bond in lactone/esters and hydroxyl bonded C) [58], while the peak at 287.4 eV can be attributed to C═O groups (carbonyl groups and carbons attached to two ether/hydroxyl groups) [59]. Finally, the peak observed at 289.1 eV corresponds to O-C═O groups in carboxyl or ester groups [57].

With respect to the O1s region (Fig. 4(e) and 4 (f)), the peaks observed at 531.3, 532.5 and 534.9 eV correspond to C═O (carbonyl oxygen of quinines), -C-O (ether and hydroxyl groups bonded to aliphatic and carbonyl shake-up) and O═C-O (oxygen atoms in carboxyl groups) groups, respectively [57,58].

Comparing the contribution of the peak areas corresponding to the C1s and O1s regions, it can be observed that the activation of the solid with KOH and its subsequent functionalization with H_2SO_4 generates a decrease in the contribution of the -C-O and O═C-O groups, while an increase in the contribution of the C═O groups is observed. The latter confirms the results obtained by FTIR. The observed reduction of surface functionalities is a consequence of the thermal and chemical treatments to which the carbons were subjected. In a previous work, Fermanelli et al. observed a significant decrease in the number of functional groups present in biomass after pyrolysis treatment at 500 °C [59], an effect attributed to the degradation and release of volatile compounds [60]. Thus, temperature is considered to be the most important parameter controlling the surface functionalities of carbons [61]. However, the use of KOH as an activating agent usually increases the carbonyl groups. As stated by Jedynak and Charmas, the amount of functional groups depends on the biomass precursor and the activating agent [62].

3.2. Crude glycerol characterization

The characterization of the crude glycerol is shown in Table 2. The results indicate that the sample presents a density similar to that of the analytical one (~1.26 g ml^{-1}) with a glycerol content of the order of 80 wt% in aqueous solution, with a water content of 12 wt%. This sample has 0.15 wt% of MeOH and 3.27 wt% of MONG. The MONG includes the non-glycerol organic matter, formed by a set of free fatty acids, oils, fats and phospholipids that come from the transesterification reaction in the production of biodiesel. They are mostly insoluble and remain as an insoluble organic phase in the aqueous phase of glycerol. These also include MeOH, but its content can be discounted since it is independently quantified. The low percentages of MeOH and MONG would indicate that this sample has a low organic matter load. The acidic

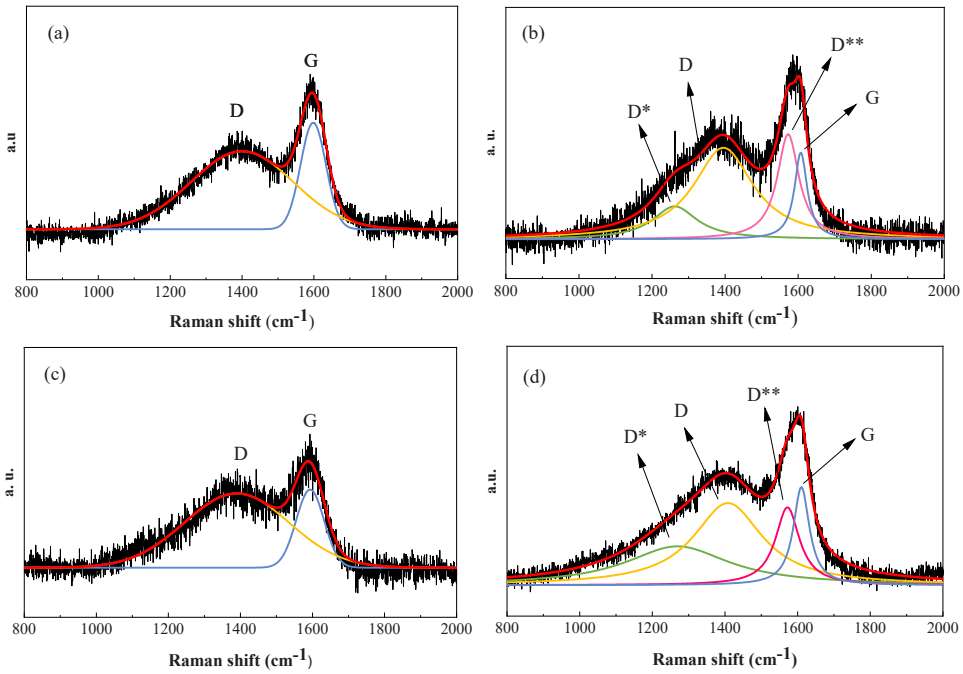

Fig. 3. Deconvoluted Raman spectra of all samples in the range 800–2000 cm^{-1}. (a) PCF; (b) APC-F; (c) PC (d) APC.

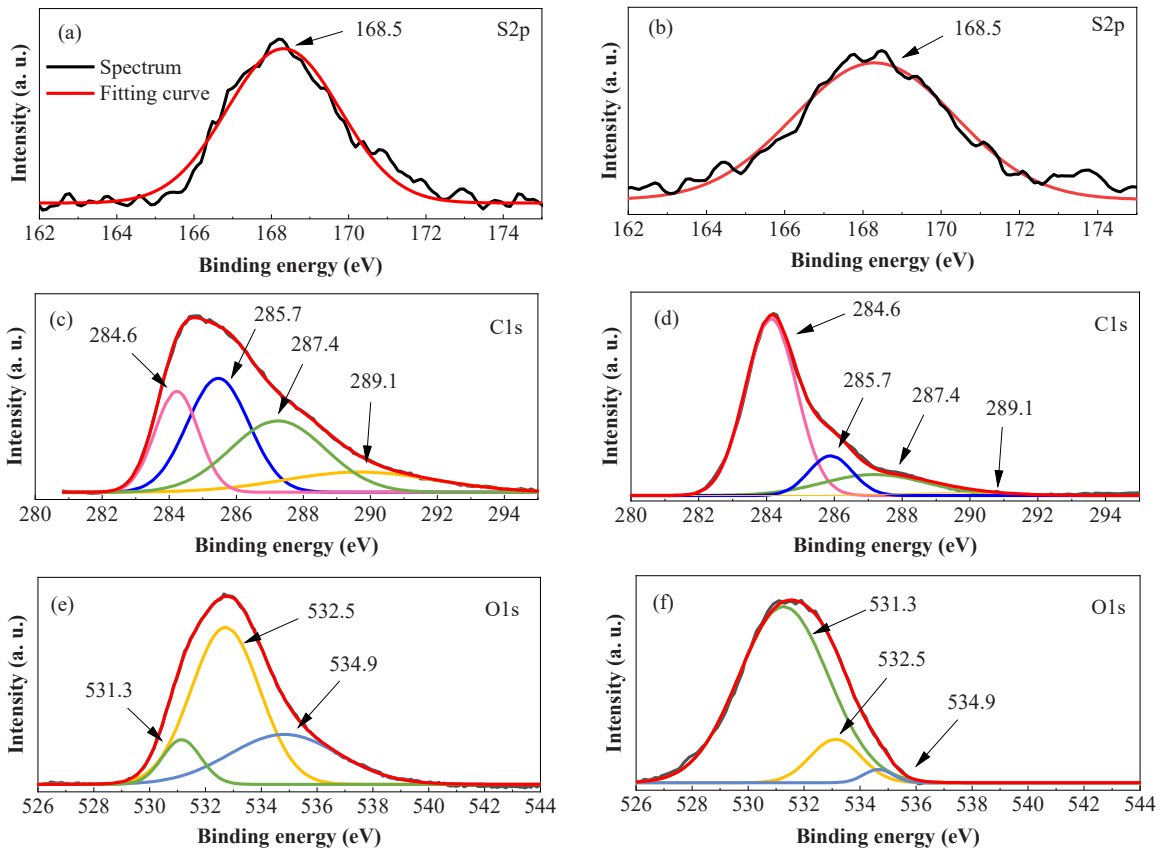

Fig. 4. X-ray photoelectron spectroscopy spectra of the solids (a) S2p region of PC-F, (b) S2p region of APC-F, (c) C1s region of PC-F, (d) C1s region of APC-F, (e) O1s region of PC-F, (f) O1s region of APC-F.

Table 2
Physicochemical properties and composition of crude glycerol.

Parameter	Value
pH	5.0
Density (g ml^{-1})	1.27
Glycerol content (wt%)	80.58
Water content (wt%)	12.00
Ash content[a] (wt%)	4.00
MeOH content (wt%)	0.15
MONG content[b] (wt%)	3.27

[a] Na_2SO_4 [b] MeOH content (%p/p) has been subtracted from the total MONG content (wt%).

pH of the sample indicates that it was neutralized after the biodiesel synthesis. The company reported that the neutralization was carried out with H_2SO_4, so that 4 wt% of its ashes are based on Na_2SO_4 generated as a result of the neutralization.

3.3. Activity tests

In order to determine an operating condition, activity tests were initially carried out without catalyst, using pure analytical glycerol and acetic acid. Fig. 5 shows the activity results as a function of time (15–120 min) for the 80–200 °C thermal range, using AA/G = 6.

In Fig. 5(a) it can be observed that the conversion increases as a function of time, as expected for liquid phase reactions in batch reactors. In addition, higher conversions are obtained at higher temperatures. These results are consistent with those previously reported by Perez et al. [63]. Since these tests were performed in the absence of catalyst, it is noteworthy that glycerol conversions of 91%, 96%, and 98% can be achieved by operating at 120, 160, and 200 °C, respectively, during 120 min

Fig. 5(b), (c) and (d) show the selectivity towards MAG, DAG and TAG as a function of time for the 80–200 °C thermal range. For the curves between 80 and 160 °C, it is observed that the selectivity towards MAG decreases with time along with an increase in DAG and TAG selectivity, suggesting the natural mechanism of glycerol esterification. At 200 °C no change in selectivity with time is observed.

According to the reaction mechanism, glycerol is initially acetylated with acetic acid to 1-MAG and 2-MAG, releasing water molecules. Then MAG continues reacting with AA forming 1,2-DAG and 1,3-DAG, and the addition of another molecule of AA to DAGs finally forms TAG (5−11) [64]. Tonutti et al. reported that, from the perspective of G, MAG, DAG and TAG, it is a serial mechanism whereas from the perspective of AA and W, it consists of three parallel reactions [65].

$$G + AA \leftrightarrow 1\text{-MAG} + W \quad (5)$$

$$G + AA \leftrightarrow 2\text{-MAG} + W \quad (6)$$

$$1\text{-MAG} + AA \leftrightarrow 1,3\text{-DAG} + W \quad (7)$$

$$1\text{-MAG} + AA \leftrightarrow 1,2\text{-DAG} + W \quad (8)$$

$$2\text{-MAG} + AA \leftrightarrow 1,2\text{-DAG} + W \quad (9)$$

$$1,3\text{-DAG} + AA \leftrightarrow TAG + W \quad (10)$$

$$1,2\text{-DAG} + AA \leftrightarrow TAG + W \quad (11)$$

From Fig. 5, it is also observed that, at low reaction times, the MAG selectivity (Fig. 5(b)) is always higher than the selectivity towards DAG (Fig. 5(c)) and TAG (Fig. 5(d)), suggesting that the first reaction steps (Eqs. (5) and (6)) are the fastest.

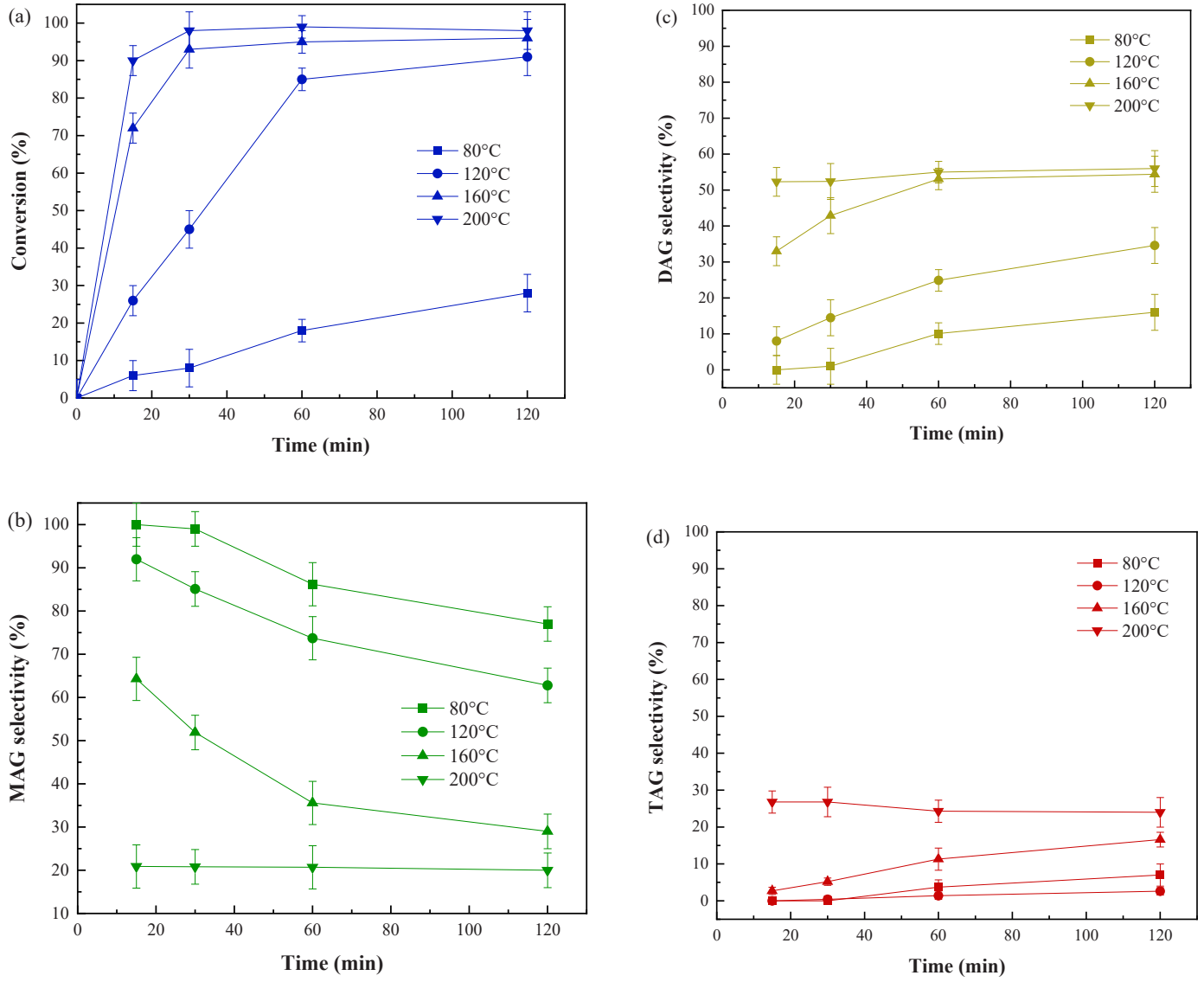

Fig. 5. (a) Glycerol conversion (b) MAG selectivity (c) DAG selectivity (d) TAG selectivity. Reaction conditions in the absence of catalyst: AA/G = 6 (molar), 80–200 °C, 15–120 min, P_{N2} = 2 MPa.

Fig. 6 shows the activity results at 120 °C and 30 min of reaction as a function of AA/G molar ratio (1−9).

As can be seen, an increase in the AA/G molar ratio between 1 and 6 causes an increase in the conversion of glycerol with an increase in the DAG selectivity, and a maintenance in the selectivity towards TAG. Since the reactions involved in the mechanism (Eqs. 5–11) are reversible, it is expected that an increase in the AA/G molar ratio would produce a shift of the equilibrium towards product formation, which would explain the increase in glycerol conversion and in the formation of DAG from MAG. Since the reactions become slower as glycerol is esterified, TAG formation from DAG is the least favored of all and, therefore, no significant changes in its selectivity are observed with increasing AA/G molar ratio. This effect has been reported by several authors in the literature using different acid solids such as polyvinylbenzene [30], sulfuric acid functionalized zirconia [66], supported heteropolyacids [67], Fe_3O_4/SiO_2-SO_4^{2-} [68] and $SbCl_5$ [69]. Since no significant changes in conversion are observed for a molar ratio of AA/G = 6 and higher, this molar ratio of reactants was selected to continue with the study of the reaction.

Fig. 7 shows the activity results as a function of time using the crude glycerol sample at 120 °C for a molar ratio AA/G = 6. The results indicate that it is possible to convert the glycerol present in the crude glycerol sample, reaching 90% conversion at 120 min. With respect to the product distribution, esterification leads mainly to the formation of MAG, with DAG and TAG being the minority products. It is also observed that as the glycerol conversion increases, the MAG selectivity decreases, accompanied by an increase in the selectivity towards DAG and TAG, following the nature of the esterification mechanism previously explained.

If the activity results of Figs. 5 and 7 are compared under the same reaction conditions (120 °C, AA/G = 6), some differences are observed when using analytical glycerol and the crude glycerol sample. These differences lie mainly in the conversion values: at 30 min, for example, conversions of 45% (analytical) and 61% (crude) are obtained.

To explain these differences, some reactions were carried out using analytical glycerol solutions by adding individually, and with a similar concentration, the impurities contained in the crude glycerol sample. Table 3 shows the results of these tests at 120 °C and 30 min, using a molar ratio AA/G = 6.

With respect to the presence of water, it is observed that the conversion decreases from 45.7% to 38% when its content is 20 wt%, indicating that water has an adverse effect on the conversion, which is

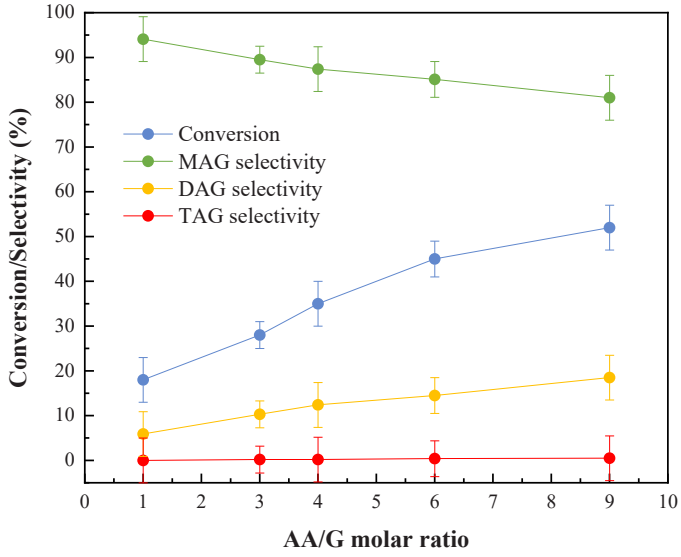

Fig. 6. Glycerol conversion and selectivity towards MAG, DAG and TAG as a function of AA/G molar ratio. Reaction conditions: AA/G = 1–9 (molar), 120 °C, P_{N2} = 2 MPa, 30 min.

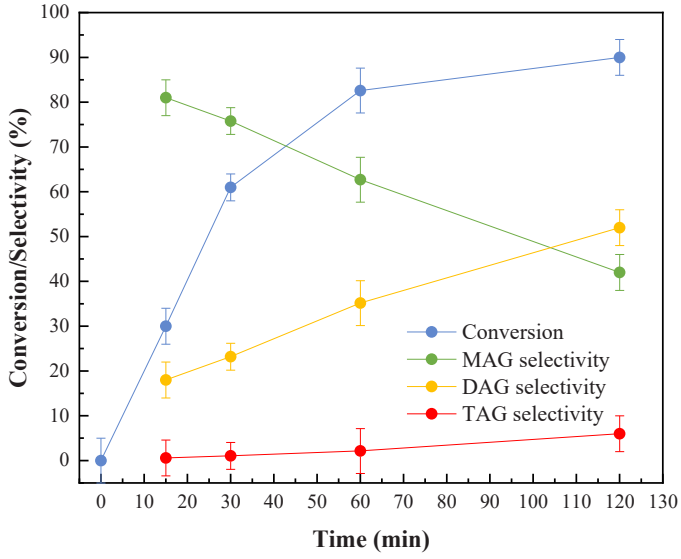

Fig. 7. Glycerol conversion and selectivity towards MAG, DAG and TAG as a function of time for industrial crude glycerol sample. Reaction conditions: AA/G = 6 (molar), 120 °C, 15–120 min, P_{N2} = 2 MPa.

expected since it is a by-product of the reaction, and its accumulation shifts the equilibrium towards product formation. The MAG selectivity, moreover, is slightly higher for the sample containing water, indicating that water decreases the formation of DAG and TAG due to the chemical equilibrium effect [63].

On the other hand, the presence of MeOH also decreases the conversion from 45.7% to 33% when its content is 20 wt%, indicating that it interferes in the glycerol esterification. The -OH group of MeOH could interfere in the esterification mechanism by reacting with acetic acid to form other esters, which was verified by chromatography, detecting the presence of methyl acetate in the reaction products.

Since the crude glycerol sample has a MONG content of 3.27%, its effect on the activity was determined using oleic acid as a model molecule. The addition of oleic acid produced practically no change in conversion and product selectivity, which would indicate that MONGs do not interfere with the reaction.

Table 3
Homogeneous liquid phase esterification using the crude glycerol sample and analytical glycerol solutions containing the impurities of the crude glycerol.

Sample	X (%)	S_{MAG} (%)	S_{DAG} (%)	S_{TAG} (%)
Crude glycerol	61.0	75.8	23.2	1.1
Analytical glycerol	45.7	85.3	14.4	0.3
Analytical glycerol + H_2O (20 wt%)	38.0	87.2	12.5	0.3
Analytical glycerol + MeOH (20 wt %)	33.0	87.9	11.8	0.3
Analytical glycerol + Oleic acid (20 wt%)	45.5	84.9	14.6	0.5
Analytical glycerol + Na_2SO_4 (10 wt %)	41.5	85.0	14.5	0.5
Analytical glycerol + H_2SO_4 (pH = 5)	58.0	78.7	20.6	0.7

Reaction conditions: 120 °C, 30 min, AA/G = 6, P_{N2} = 2 MPa

If the crude glycerol sample is compared with the analytical sample, it is observed that the former shows a higher conversion than the latter. Since crude glycerol presents H_2O and MeOH, whose effects are adverse, the presence of Na_2SO_4 could be the one that generates the positive effect on the activity. However, when tests are carried out with analytical glycerol and adding 10 wt% of Na_2SO_4 with respect to glycerol, a conversion similar to that obtained with analytical glycerol is attained, indicating that the presence of the salt does not affect the activity levels. Since crude glycerol has a pH = 5, the excess of H_2SO_4 during neutralization could be responsible for the increase in activity. Tests using analytical glycerol and H_2SO_4 at pH = 5 show an increase in conversion from 45.7% to 58%, confirming this hypothesis.

To improve the activity levels, reaction tests were carried out with the crude glycerol sample in the presence of the carbons synthesized from peanut shells and those functionalized with H_2SO_4. The results of conversion and products selectivity are shown in Fig. 8. The carbon balance in all cases is in the range 85–100%.

Firstly, it is important to note that, when PC and APC starting materials were used as catalysts, the conversion and selectivity in both cases are similar to those obtained in the absence of catalyst. This result can be attributed to the low number of acid sites and the low acid strength of the sites present in both solids, as demonstrated by potentiometric titration (Table 1).

The results in Fig. 8(a) show that glycerol conversion increases with time using PC-F and APC-F carbons. Compared to the homogeneous reaction, both solids show higher conversions, with APC-F being more active than PC-F. This behavior can be attributed to the combination of the acidity of the solids and their textural properties. Both solids have very strong acid sites (Ei > 100 mV), but the APC-F catalyst has a significantly higher specific surface area, which could favor the esterification mechanism [63].

With respect to product distribution, the solids PC-F and APC-F present the lowest selectivity values to MAG, showing a higher tendency to form DAG and TAG. This is in agreement with the activity trend shown: by converting glycerol completely in shorter times, both solids begin to consume MAG to form DAG and TAG. The results indicate that by employing the APC-F catalyst, it is possible to obtain complete conversion of glycerol and selectivities to MAG, DAG and TAG of 29.4%, 54.1% and 16.5%, respectively, operating at 120 °C with a molar ratio AA/G = 6 and a mass ratio C/G = 0.25. Similar results were obtained by other authors employing analytical glycerol and using carbons from different biomass sources such as rice husks (TC-L) [31], Karanja seed husks (KJ-400) [33], wastewater (SC) [70], glycerol (C-glycerol) [71], sucrose ($C_{SBA\text{-}15}$-BDS) [72] and catkins from willow (WCS) [73]. The best activity results for these solids are reported in Table 4, together with the reaction conditions under which they were evaluated. The results obtained in this work are included in the table for direct comparison. The results using the catalyst synthesized in this work are promising

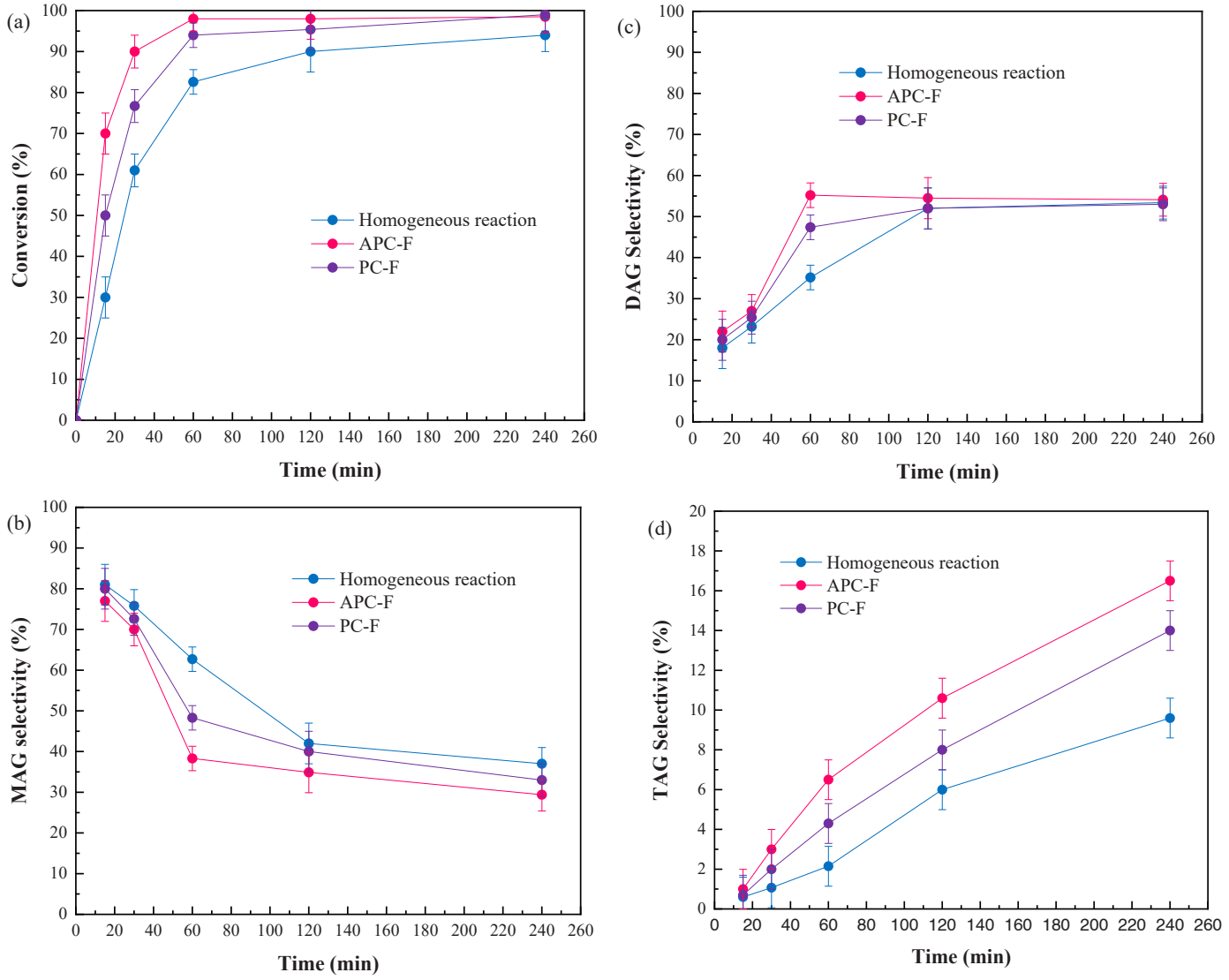

Fig. 8. (a) Glycerol conversion (b) MAG selectivity (c) DAG selectivity (d) TAG selectivity. Reaction conditions: AA/G = 6 (molar), 120 °C, 15–240 min, P_{N2} = 2 MPa.

Table 4
Carbons used as catalysts in the esterification reaction of glycerol with acetic acid.

Catalyst	T (°C)	AA/G	t (h)	C/G	X (%)	S (%)			Ref.
						MAG	DAG	TAG	
KJ-400	120	5	4.0	0.08	90.0	56.0	40.0	4.0	[33]
TC-L	150	5	5.0	0.05	90.0	10.0	90.0 (*)		[31]
SC	120	6	6.0	0.16	90.8	46.9	48.4	6.3	[70]
APC-F	120	6	4.0	0.25	99.0	29.4	54.1	16.5	This work
C-glycerol	110	6	2.0	0.10	96.0	26.0	56.0	18.0	[71]
C_{SBA-15}-BDS	120	6	24.0	0.09	98.0	16.0	54.0	30.0	[72]
WCS	120	5	5.0	0.07	98.0	5.0	50.0	45.0	[73]
AC micro_BDS	110	6.0	1.0	0.09	~100.0	8.0	50.0	42.0	[74]
Y_2O_3/PKS-T700	130	12.0	5.0	0.10	~100.0	11.1	60.2	29.6	[75]

(*) Selectivity towards (DAG + TAG).

compared to those reported by other authors, due to the simplicity of its synthesis and the fact that crude glycerol has been used as a reagent.

To study the reusability of the material, successive reaction cycles of 120 min each were carried out at 120 °C, using a molar ratio AA/G = 6 and a mass ratio C/G = 0.25. After each cycle, and before a new one, the catalyst was washed with distilled water several times and dried in an oven at 105 °C for 24 h. The activity results are shown in Fig. 9.

As observed in Fig. 9, the catalyst maintains its activity after five reaction cycles, with slight changes in selectivity towards the most substituted products. The TAG selectivity decreases slightly from 11% to 8.7% and the selectivity towards DAG from 55.5% to 54.2%, with an increase in the MAG selectivity from 33.4% to 37.1%.

It is noteworthy that an increase in the mass of dry solid of the order of 176% was observed between the first and third reaction cycles,

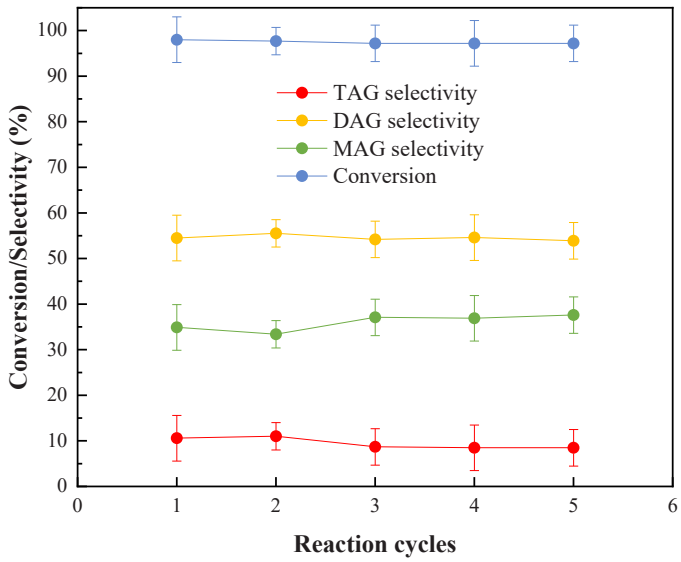

Fig. 9. Activity results using the solid APC-F in different reaction cycles (a) Glycerol conversion (b) MAG selectivity (c) DAG selectivity (d) TAG selectivity. Reaction conditions: AA/G = 6 (molar), C/G = 0.25 (mass), 120 °C, 120 min, P_{N2} = 2 MPa.

remaining constant in the fourth and fifth ones. In addition, the carbon balance obtained after the fifth use was ~115%, which would indicate the possible adsorption of chemical species on the catalyst surface. On the other hand, the product solution became colorless after each cycle, indicating that the carbon could adsorb part of the impurities contained in the crude glycerol sample. To corroborate these hypotheses, the used catalyst sample was characterized by BET analysis, XRD and potentiometric titration. The BET results indicated a decrease in the specific surface area of the carbon from 918 $m^2\ g^{-1}$ to 307 $m^2\ g^{-1}$ (Table 1), with a decrease in total pore volume from 0.30 $cm^3\ g^{-1}$ to 0.10 $cm^3\ g^{-1}$, which would indicate a surface coverage of the carbon and partial blockage of pores. The X-ray diffraction of the sample used (Fig. 10) determined the presence of characteristic peaks of Na_2SO_4 (JCPDS 00–001-1000), indicating that the carbon adsorbed this impurity, which would be responsible for the decrease in specific surface area and pore blockage observed.

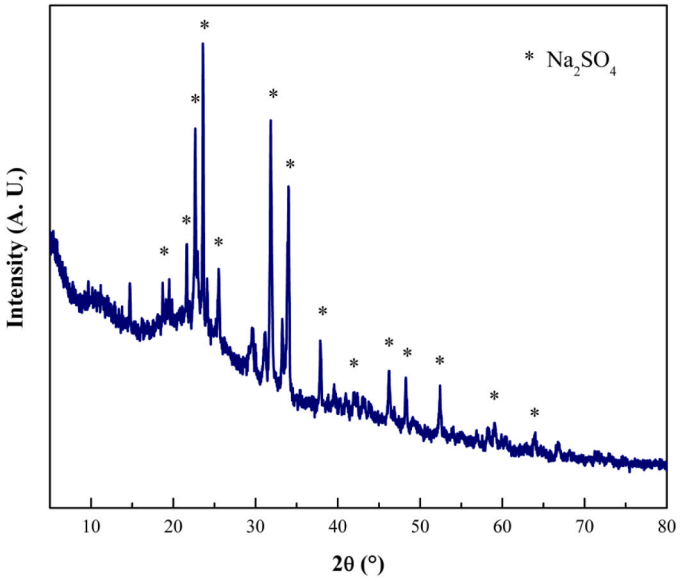

Fig. 10. Diffractogram of the APC-F catalyst used after 5 cycles.

The potentiometric titration results showed a slight decrease in the total number of acid sites, without losing their acidic strength, which would explain the slight decrease in selectivity towards DAG and TAG observed after the first reaction cycles. However, the activity results are promising and indicate that after five reaction cycles, the acid sites are still very strong and the total number of sites varies slightly, demonstrating the stability of the catalyst.

4. Conclusions and prospects

In this work, carbons obtained from peanut shells discarded from the industrial process and functionalized with sulfuric acid were evaluated as catalysts in the esterification reaction of crude glycerol with acetic acid.

For this purpose, the best operating conditions were determined without using catalyst, using analytical glycerol and varying the reaction time (15–120 min), temperature (80–200 °C) and different AA/G molar ratios (1−9). At 120 °C and using a molar ratio AA/G = 6, the reaction in homogeneous phase was evaluated using crude glycerol obtained in the biodiesel synthesis, which presented acid pH, and water, methanol and Na_2SO_4 as main impurities, in addition to non-glycerol organic matter (MONG). Since crude glycerol was more active in the esterification reaction than analytical glycerol, tests were carried out to determine the origin of these differences. By analyzing the impurities of the crude glycerol individually it was determined that Na_2SO_4 and MONG do not alter the catalytic performance, but both water and methanol decrease the activity levels. The acidity of the crude glycerol (pH = 5) due to the presence of H_2SO_4 product of its neutralization improves the catalytic activity, increasing the conversion levels.

In order to improve the activity levels, catalysts were prepared based on carbon obtained by pyrolysis of peanut shells (PC), activated by a treatment with KOH (APC) and functionalized with H_2SO_4 (PC-F and APC-F, respectively). The textural and acidity characterization results showed that the functionalized materials (PC-F and APC-F) present a higher specific surface area and total pore volume than the starting materials (PC and APC). Furthermore, they showed a higher number of acid sites and a higher acid strength. By the Fourier Transform Infrared spectroscopy and X-ray photoelectron spectroscopy techniques it was determined that both PC-F and APC-F present -HSO_3 groups covalently attached to the carbonaceous structure, indicating that the H_2SO_4 functionalization treatment was effective in generating acidic groups on the carbons.

Compared to the esterification in homogeneous phase, both solids present higher conversions, with APC-F being more active than PC-F. This behavior can be attributed to the combination of the acidity of the solids and their textural properties.

After 5 reaction cycles at 120 °C, using a molar ratio AA/G and a mass ratio C/G = 0.25, the catalyst showed a decrease in specific surface area and total pore volume due to a surface coverage and partial blockage of pores because of the adsorption of Na_2SO_4 present in the crude glycerol. However, the solid was able to maintain activity levels showing 100% glycerol conversion with MAG, DAG and TAG selectivities of 55%, 35% and 10%, respectively.

This study demonstrates the activity and stability of functionalized carbon-based catalysts derived from biomass in the esterification reaction of glycerol with acetic acid. The practical implications of this study lie in the use of crude glycerol as the reagent, which significantly reduces the production costs of acetylglycerols associated with glycerol refining. In addition, the catalysts were synthesized from pyrolytic carbon derived from peanut shell waste, thus closing the carbon cycle. Furthermore, it is important to mention that the reaction products solution is colorless, while the crude glycerol has a brownish color, suggesting that the catalyst also acts as an adsorbent for certain impurities.

Future research should include kinetic studies for simulating and designing the chemical reactor. In addition, to carry out an exhaustive study of the process, it is necessary to perform technical-economic

analyses, as well as energetic, exergetic and CO_2 emission studies.

Declaration of Competing Interest

None.

Acknowledgements

This work was made posible thanks to the funding received from "Consejo Nacional de Investigaciones Científicas y Técnicas" (CONICET-PIP 0386), "Universidad Nacional de La Plata" (UNLP-I248) and "Universidad Tecnológica Nacional" (MSTCCO0008681TC).

References

[1] Fundación Leia Centro de Desarrollo Tecnológico, "Observatorio Industrial del Sector Químico. Bioplásticos," no. January, p. 123, 2007.
[2] C.J.A. Mota, B.P. Pinto, A.L. de Lima, Glycerol: A Versatile Renew. Feedstock Chem. Ind. (2017).
[3] I.N. Buffoni, M.N. Gatti, G.F. Santori, F. Pompeo, N.N. Nichio, Hydrogen from glycerol steam reforming with a platinum catalyst supported on a SiO_2-C composite, Int. J. Hydrog. Energ. 42 (2017) 12967–12977, https://doi.org/10.1016/j.ijhydene.2017.04.047.
[4] F.M. Perez, G.F. Santori, F. Pompeo, N.N. Nichio, Silica-resin-bentonite nanocomposite and its application in catalysis, Minerals 12 (2022) 1486, https://doi.org/10.3390/min12121486.
[5] M.N. Gatti, N.N. Nichio, F. Pompeo, Advances for biorefineries: glycerol hydrogenolysis to 1,3-propylene glycol, Reactions 3 (2022) 451–498, https://doi.org/10.3390/reactions3030032.
[6] M.N. Gatti, F.M. Perez, G.F. Santori, N.N. Nichio, F. Pompeo, Heterogeneous Catalysts for Glycerol Biorefineries: Hydrogenolysis to 1,2-Propylene Glycol, Materials 16 (2023) 3551, https://doi.org/10.3390/ma16093551.
[7] R. Sedghi, H. Shahbeik, H. Rastegari, S. Rafiee, W. Peng, A. Nizami, V.K. Gupta, W. Chen, S.Shiung Lam, J. Pan, M. Tabatabaei, M. Aghbashlo, Turning biodiesel glycerol into oxygenated fuel additives and their effects on the behavior of internal combustion engines: A comprehensive systematic review, Renew. Sustain. Energy Rev. 167 (2022) 112805, https://doi.org/10.1016/j.rser.2022.112805.
[8] X. Liao, Y. Zhu, S.G. Wang, H. Chen, Y. Li, Theoretical elucidation of acetylating glycerol with acetic acid and acetic anhydride, Appl. Catal. B Environ. 94 (2010) 64–70, https://doi.org/10.1016/j.apcatb.2009.10.021.
[9] G. Triacetate, T. Cosmetic, I. Review, E. Panel, C.I.R.E. Panel, Final Report on the Safety Assessment of Triacetin, Int. J. Toxicol. 22 (2) (2003) 1–10, https://doi.org/10.1080/10915810390204845.
[10] G.P. Romanelli, D.M. Ruiz, G.A. Pasquale, "Capítulo 3. Biomasa,", Quím. la biomasa Y. los biocombustibles (2017) 39–47.
[11] P. Ning, G. Yang, L. Hu, J. Sun, L. Shi, Y. Zhou, Z. Wang, J. Yang, Recent advances in the valorization of plant biomass, Biotechnol. Biofuels 14 (1) (2021) 1–22, https://doi.org/10.1186/s13068-021-01949-3.
[12] L.G. Wade, 2011. Whitman College, Organic Chemistry, Eighth Edition, Pearson, México.
[13] Y. Sun, J. Hu, S. An, Q. Zhang, Y. Guo, D. Song, Q. Shang, Selective esterification of glycerol with acetic acid or lauric acid over rod-like carbon-based sulfonic acid functionalized ionic liquids, Fuel 207 (2017) 136–145, https://doi.org/10.1016/j.fuel.2017.06.073.
[14] C.E. Goncalves, L.O. Laier, M.J. da Silva, Novel Esterification of Glycerol Catalysed by Tin Chloride (II): A Recyclable and Less Corrosive Process for Production of Bio-Additives, Catal. Lett. 141 (2011) 1111–1117, https://doi.org/10.1007/s10562-011-0570-x.
[15] Y. Liu, E. Lotero, J.G. Jr. Goodwin, Effect of water on sulfuric acid catalyzed esterification, J. Molec. Cat. A: Chem. 245 (2006) 132–140, https://doi.org/10.1016/j.molcata.2005.09.049.
[16] B. Meireles, V.L.P. Pereira, Synthesis of Bio-Additives: Transesterification of Ethyl Acetate with Glycerol Using Homogeneous or Heterogeneous Acid Catalysts, J. Braz. Chem. Soc. 24 (2013) 17–25, https://doi.org/10.1590/S0103-50532013000100004.
[17] M.S. Khayoon, B.H. Hameed, Acetylation of glycerol to biofuel additives over sulfated activated carbon catalyst, Biores. Technol. 102 (2011) 9229–9235, https://doi.org/10.1016/10.1016/j.biortech.2011.07.035.
[18] P.S. Kong, P.S. M.K, M.W.M.A.W. Aroua, H.V. Daud, P. Lee, Y.Peresc Cognetc, Catalytic role of solid acid catalysts in glycerol acetylation for the production of bio-additives: a review, RSC Adv. 6 (2016) 68885, https://doi.org/10.1039/C6RA10686B.
[19] J. Lilja, D.Y. Murzin, T. Salmi, J. Aumo, P. Mäki-Arvela, M. Sundell, Esterification of different acids over heterogeneous and homogeneous catalysts and correlation with the Taft equation, J. Molec. Cat. A: Chem. 182-183 (2002) 555–563, https://doi.org/10.1016/S1381-1169(01)00495-2.
[20] Y. Jiang, X. Li, H. Zhao, Z. Hou, Esterification of glycerol with acetic acid over SO_3H-functionalized phenolic resin, Fuel 255 (2019) 115842, https://doi.org/10.1016/j.fuel.2019.115842.
[21] S. Kale, S.B. Umbarkar, M.K. Dongare, R. Eckelt, U. Armbruster, A. Martin, Selective formation of triacetin by glycerol acetylation using acidic ion-exchange resins as catalyst and toluene as an entrainer, Appl. Catal. A 490 (2015) 10–16, https://doi.org/10.1016/j.apcata.2014.10.059.
[22] V.L.C. Gonçalves, B.P. Pinto, J.C. Silva, C.J.A. Mota, Acetylation of Glycerol Catalyzed by Different Solid Acids, Catal. Today 133-135 (2008) 673–677, https://doi.org/10.1016/j.cattod.2007.12.037.
[23] N.J. Venkatesha, Y.S. Bhat, B.S.J. Prakash, Volume Accessibility of Acid Sites in Modified Montmorillonite and Triacetin Selectivity in Acetylation of Glycerol, RSC Adv. 6 (2016) 45819–45828, https://doi.org/10.1039/c6ra05720a.
[24] W. Hu, Y. Zhang, Y. Huang, J. Wang, J. Gao, J. Xu, Selective esterification of glycerol with acetic acid to diacetin using antimony pentoxide as reusable catalyst, J. Energy Chem. 24 (2015) 632–636, https://doi.org/10.1016/j.jechem.2015.08.00.
[25] A. Patel, S. Singh, A green and sustainable approach for esterification of glycerol using 12-tungstophosphoric acid anchored to different supports: kinetics and effect of support, Fuel 118 (2014) 358–364, https://doi.org/10.1016/j.fuel.2013.11.005.
[26] B.O. Dalla Costa, H.P. Decolatti, M.S. Legnoverde, C.A. Querini, Influence of acidic properties of different solid acid catalysts for glycerol acetylation, Cat. Today 289 (2017) 222–230, https://doi.org/10.1016/j.cattod.2016.09.015.
[27] Foreign Agricultural Service, U. S. Department of Agriculture. https://ipad.fas.usda.gov/cropexplorer/cropview/commodityView.aspx?cropid=2221000, 2023 (accessed June 2023).
[28] H. Shahbeik, S. Rafiee, A. Shafizadeh, D. Jeddi, T. Jafary, S.S. Lam, J. Pan, M. Tabatabaei, M. Aghbashlo, Characterizing sludge pyrolysis by machine learning: Towards sustainable bioenergy production from wastes, Renew. Energy 199 (2022) 1078–1092, https://doi.org/10.1016/j.renene.2022.09.022.
[29] H. Li, J. Chen, W. Zhang, H. Zhan, C. He, Z. Yang, H. Peng, L. Leng, Machine-learning-aided thermochemical treatment of biomass: a review, Biofuel Res. J. 37 (2023) 1786–1809, https://doi.org/10.18331/BRJ2023.10.1.4.
[30] R. Mou, X. Wang, Z. Wang, D. Zhang, Z. Yin, Y. Lv, Z. Wei, Synthesis of fuel bioadditive by esterification of glycerol with acetic acid over hydrophobic polymer-based solid acid, Fuel 302 (2021) 121175, https://doi.org/10.1016/j.fuel.2021.121175.
[31] T.S. Galhardo, N. Simone, M. Gonçalves, F.C.A. Figueiredo, D. Mandelli, W. A. Carvalho, Preparation of sulfonated carbons from rice husk and their application in catalytic conversion of glycerol, ACS Sustain. Chem. Eng. 1 (2013) 1381–1389, https://doi.org/10.1021/sc400117t.
[32] U.I. Nda-Umar, I. Ramli, E.N. Muhamad, Y.H. Taufiq-Yap, N. Azri, Synthesis and Characterization of Sulfonated Carbon Catalysts Derived from Biomass Waste and Its Evaluation in Glycerol Acetylation, Biomass-.-. Convers. Biorefinery 12 (2022) 2045–2060, https://doi.org/10.1007/s13399-020-00784-0.
[33] J.Mahammad Rafi, A. Rajashekar, M. Srinivas, B.V.S.K. Rao, R.B.N. Prasad, N. Lingaiah, Esterification of Glycerol over a Solid Acid Biochar Catalyst Derived from Waste Biomass, RSC Adv. 5 (2015) 44550–44556, https://doi.org/10.1039/C5RA06613A.
[34] M.L. Tao, H.Y. Guan, X.H. Wang, Y.C. Liu, R.F. Louh, Fabrication of Sulfonated Carbon Catalyst from Biomass Waste and Its Use for Glycerol Esterification, Fuel Process. Technol. 138 (2015) 355–360, https://doi.org/10.1016/j.fuproc.2015.06.021.
[35] F. Ma, M.A. Hanna, Biodiesel production: a review, Bioresour. Technol. 70 (1999) 1–15, https://doi.org/10.1016/s0960-8524(99)00025-5.
[36] M.N. Gatti, F. Pompeo, N.N. Nichio, G.F. Santori, Crude Glycerol Hydrogenolysis to Bio-Propylene Glycol: Effect of Its Impurities on Activity, Selectivity and Stability, Processes 11 (2023) 1731, https://doi.org/10.3390/pr11061731.
[37] M. Balaraju, V. Rekha, B.L.A. Prabhavathi Devi, R.B.N. Prasad, P.S. Sai Prasad, N. Lingaiah, Surface and structural properties of titania-supported Ru catalysts for hydrogenolysis of glycerol, Appl. Catal. A: Gen. 384 (2010) 107–114, https://doi.org/10.1016/j.apcata.2010.06.013.
[38] M. Ju, P. Rao, L. Yan, D. Gu, G. Li, Q. Chen, S. Liu, Z. Zeng, M. Zhang, W. Zhang, Synergistic adsorption and degradation of sulfamethazine by tobacco stalk-derived activated biochar: Preparation, mechanism insight and application, J. Environ. Chem. Eng. 11 (2023) 110265, https://doi.org/10.1016/j.jece.2023.110265.
[39] Z. Lu, H. Zhang, A. Shahab, K. Zhang, H. Zeng, A. Bacha, I. Nabi, H. Ullah, Comparative study on characterization and adsorption properties of phosphoric acid activated biochar and nitrogen-containing modified biochar employing Eucalyptus as a precursor, J. Clean. Prod. 303 (2021) 127046, https://doi.org/10.1016/j.jclepro.2021.127046.
[40] Z. Wei, D. Xiong, P. Duan, S. Ding, Y. Li, L. Li, P. Niu, X. Chen, Preparation of Carbon-Based Solid Acid Catalysts Using Rice Straw Biomass and Their Application in Hydration of α-Pinene, Catalysts 10 (2) (2020) 213, https://doi.org/10.3390/catal10020213.
[41] Z. Wei, G. Wei, H. Che, D. Xiong, L. Zhang, R. Xue, Y. Tang, X. Lu, A novel carbon-based solid acid catalyst with high acidity for the hydration of α-pinene to α-terpineol: Effect of graphite crystallite size and synergistic effect of defects, Mol. Catal. 552 (2024) 113631, https://doi.org/10.1016/j.mcat.2023.113631.
[42] R. Cid, G. Pecchi, Potentiometric method for determining the number and relative strength of acid sites in colored catalysts, Appl. Catal. 14 (1985) 15–21, https://doi.org/10.1016/S0166-9834(00)84340-7.
[43] B. Belhamdi, Z. Merzougui, H. Laksaci, M. Trari, The removal and adsorption mechanisms of free amino acid l-tryptophan from aqueous solution by biomass-based activated carbon by H_3PO_4 activation: Regeneration study, Phys. Chem. Earth, Parts A/B/C. 114 (2019) 102791, https://doi.org/10.1016/j.pce.2019.07.004.
[44] B. Zhang, M. Gao, W. Tang, X. Wang, C. Wu, Q. Wang, H. Xie, Reduced surface sulphonic acid concentration Alleviates carbon-based solid acid catalysts deactivation in biodiesel production, Energy 271 (2023) 127079, https://doi.org/10.1016/j.energy.2023.127079.

[45] C.H. Chia, B. Gong, S.D. Joseph, C.E. Marjo, P. Munroe, A.M. Rich, Imaging of mineral-enriched biochar by FTIR, Raman and SEM–EDX, Vib. Spectrosc. 62 (2012) 248–257, https://doi.org/10.1016/j.vibspec.2012.06.006.
[46] M. Kačuráková, R.H. Wilson, Developments in mid-infrared FT-IR spectroscopy of selected carbohydrates, Carbohydr. Polym. 44 (2001) 291–303, https://doi.org/10.1016/S0144-8617(00)00245-9.
[47] P. Verma, A. Daverey, K. Arunachalam, Development and characterization of novel low-cost engineered pine needle biochar and montmorillonite clay-based proton exchange membrane for microbial fuel cell, J. Water Process Eng. 53 (2023) 103750, https://doi.org/10.1016/j.jwpe.2023.103750.
[48] J. Xu, J. Liu, X. Zhang, P. Ling, K. Xu, L. He, S. Su, Y. Wang, S. Hu, J. Xiang, Chemical imaging of coal in micro-scale with Raman mapping technology, Fuel 264 (2020) 116826, https://doi.org/10.1016/j.fuel.2019.116826.
[49] R. Potnuri, C.S. Rao, D.V. Surya, V. Sridevi, A. Kulkarni, Two-step synthesis of biochar using torrefaction and microwave-assisted pyrolysis: Understanding the effects of torrefaction temperature and catalyst loading, J. Anal. Appl. Pyrolysis 175 (2023) 106191, https://doi.org/10.1016/j.jaap.2023.106191.
[50] J. Xu, J. Liu, P. Ling, X. Zhang, K. Xu, L. He, Y. Wang, S. Su, S. Hu, J. Xiang, Raman spectroscopy of biochar from the pyrolysis of three typical Chinese biomasses: A novel method for rapidly evaluating the biochar property, Energy 202 (2020) 117644, https://doi.org/10.1016/j.energy.2020.117644.
[51] S. Potgieter-Vermaak, N. Maledi, N. Wagner, J.H.P. Van Heerden, R. Van Grieken, J.H. Potgieter, Raman spectroscopy for the analysis of coal: a review, J. Raman Spectrosc. 42 (2011) 123–129, https://doi.org/10.1002/jrs.2636.
[52] A. Kaniyoor, S. Ramaprabhu, A Raman spectroscopic investigation of graphite oxide derived graphene, AIP Adv. 2 (2012) 032183, https://doi.org/10.1063/1.4756995.
[53] V. Harnchana, S. Chaiyachad, S. Pimanpang, C. Saiyasombat, P. Srepusharawoot, V. Amornkitbamrung, Hierarchical Fe_3O_4-reduced graphene oxide nanocomposite grown on NaCl crystals for triiodide reduction in dye-sensitized solar cells, Sci. Rep. 9 (2019) 1494, https://doi.org/10.1038/s41598-018-38050-z.
[54] L. Adams, A. Oki, T. Grady, H. McWhinney, Z. Luo, Preparation and characterization of sulfonic acid-functionalized single-walled carbon nanotubes, Phys. E: Low. -Dimens. Syst. Nanostruct. 41 (2009) 723–728, https://doi.org/10.1016/j.physe.2008.11.018.
[55] L.J. Konwar, Mäki-Arvela, J. Mikkola, SO_3H-containing functional carbon materials: synthesis, structure, and acid catalysis, Chem. Rev. 119 (2019) 11576–11630, https://doi.org/10.1021/acs.chemrev.9b00199.
[56] A. Malaika, D. Mesjasz, M. Kozłowski, Maximizing the selectivity to triacetin in glycerol acetylation through a plastic waste-derived carbon catalyst development and selection of a reaction unit, Fuel 333 (2023) 126271, https://doi.org/10.1016/j.fuel.2022.126271.
[57] Y. Zhao, D. Feng, Y. Zhang, Y. Huang, S. Sun, Effect of pyrolysis temperature on char structure and chemical speciation of alkali and alkaline earth metallic species in biochar, Fuel Process. Technol. 141 (2016) 54–60, https://doi.org/10.1016/j.fuproc.2015.06.029.
[58] M. Smith, L. Scudiero, J. Espinal, J. McEwen, M. Garcia-Perez, Improving the deconvolution and interpretation of XPS spectra from chars by ab initio calculations, Carbon 110 (2016) 155–171, https://doi.org/10.1016/j.carbon.2016.09.012.
[59] C.S. Fermanelli, A. Córdoba, L.B. Pierella, C. Saux, Pyrolysis and copyrolysis of three lignocellulosic biomass residues from the agro-food industry: A comparative study, Waste Manag. 102 (2020) 362–370, https://doi.org/10.1016/j.wasman.2019.10.057.
[60] F. Meng, J. Yu, A. Tahmasebi, Y. Han, H. Zhao, J. Lucas, T. Wall, Characteristics of Chars from Low-Temperature Pyrolysis of Lignite, Energy Fuels 28 (1) (2014) 275–284, https://doi.org/10.1021/ef401423s.
[61] J. Singh, S. Basu, H. Bhunia, CO_2 capture by modified porous carbon adsorbents: Effect of various activating agents, J. Taiwan Inst. Chem. Eng. 102 (2019) 438–447, https://doi.org/10.1016/j.jtice.2019.06.011.
[62] K. Jedynak, B. Charmas, Adsorption properties of biochars obtained by KOH activation, Adsorption (2023), https://doi.org/10.1007/s10450-023-00399-7.
[63] F.M. Perez, M.N. Gatti, N.N. Nichio, F. Pompeo, Bio-additives from glycerol acetylation with acetic acid: Chemical equilibrium model, Results Eng. 15 (2022) 100502, https://doi.org/10.1016/j.rineng.2022.100502.
[64] S. Zhu, X. Gao, F. Dong, Y. Zhu, H. Zheng, Y. Li, Design of a highly active silver-exchanged phosphotungstic acid catalyst for glycerol esterification with acetic acid, J. Catal. 306 (2013) 155–163, https://doi.org/10.1016/j.jcat.2013.06.026.
[65] L.G. Tonutti, B.O. Dalla Costa, H.P. Decolatti, G. Mendow, C.A. Querini, Determination of kinetic constants for glycerol acetylation by particle swarm optimization algorithm, Chem. Eng. J. 424 (2021) 130408, https://doi.org/10.1016/j.cej.2021.130408.
[66] P.S. Reddy, P. Sudarsanam, G. Raju, B.M. Reddy, Selective acetylation of glycerol over CeO_2-M and SO_4^{2-}/CeO_2-M (M = ZrO_2 and Al_2O_3) catalysts for synthesis of bio additives, J. Ind. Eng. Chem. 18 (2012) 648–654, https://doi.org/10.1016/j.jiec.2011.11.063.
[67] S. Magar, G.T. Mohanraj, S.K. Jana, C.V. Rode, Synthesis and characterization of supported heteropoly acid: Efficient solid acid catalyst for glycerol esterification to produce biofuel additives, Inorg. Nano-Met. Chem. 50 (2020) 1157–1165, https://doi.org/10.1080/24701556.2020.1737817.
[68] K. Abida, B. Chudasama, A. Ali, Development and functionalization of magnetic nanoparticles as stable and reusable catalysts for triacetin synthesis, N. J. Chem. 44 (2020) 9365–9376, https://doi.org/10.1039/D0NJ00488J.
[69] F.M.R.S. Altino, D.S. da Silva, J.H. Bortoluzzi, S.M.P. Meneghetti, Investigation of glycerol acetylation in the presence of Sb catalysts, Biomass-.-. Convers. Biorefinery 13 (2023) 3237–3246, https://doi.org/10.1007/s13399-021-01318-y.
[70] M. Bartoli, C. Zhu, M. Chae, D.C. Bressler, Glycerol Acetylation Mediated by Thermally Hydrolysed Biosolids-Based Material, Catalysts 10 (2020) 5, https://doi.org/10.3390/catal10010005.
[71] A. Malaika, K. Ptaszyńska, M. Kozłowski, Conversion of Renewable Feedstock to Bio-Carbons Dedicated for the Production of Green Fuel Additives from Glycerol, Fuel 288 (2021) 119609, https://doi.org/10.1016/j.fuel.2020.119609.
[72] J. Goscianska, A. Malaika, A facile post-synthetic modification of ordered mesoporous carbon to get efficient catalysts for the formation of acetins, Catal. Today 357 (2020) 84–93, https://doi.org/10.1016/j.cattod.2019.02.049.
[73] M.L. Tao, H.Y. Guan, X.H. Wang, Y.C. Liu, R.F. Louh, Fabrication of sulfonated carbon catalyst from biomass waste and its use for glycerol esterification, Fuel Process. Technol. 138 (2015) 355–360, https://doi.org/10.1016/j.fuproc.2015.06.021.
[74] A. Malaika, D. Mesjasz, M. Kozłowski, Maximizing the selectivity to triacetin in glycerol acetylation through a plastic waste-derived carbon catalyst development and selection of a reaction unit, Fuel 333 (2023) 126271, https://doi.org/10.1016/j.fuel.2022.126271.
[75] A.F. Uchenna, R. Irmawati, Y.H. Taufiq-Yap, S.M. Izham, U.I. Nda-Umar, Glycerol acetylation over yttrium oxide (Y_2O_3) catalyst supported on palm kernel shell-derived carbon and parameters optimization studies using response surface methodology (RSM), Arab. J. Chem. 16 (2023) 104865, https://doi.org/10.1016/j.arabjc.2023.104865.